PROCEEDINGS B

royalsocietypublishing.org/journal/rspb

Research

Cite this article: Xiang K-L, Erst AS, Yang J, Peng H-W, Ortiz R del C, Jabbour F, Erst TV, Wang W. 2021 Biogeographic diversification of *Eranthis* (Ranunculaceae) reflects the geological history of the three great Asian plateaus. *Proc. R. Soc. B* **288**: 20210281. https://doi.org/10.1098/rspb.2021.0281

Received: 2 February 2021
Accepted: 11 March 2021

Subject Category:
Ecology

Subject Areas:
ecology, evolution

Keywords:
Asia, biogeography, Cenozoic, phylogeny, Ranunculaceae, tectonic evolution

Author for correspondence:
Wei Wang
e-mail: wangwei1127@ibcas.ac.cn

Electronic supplementary material is available online at https://doi.org/10.6084/m9.figshare.c.5355027.

THE ROYAL SOCIETY PUBLISHING

Biogeographic diversification of *Eranthis* (Ranunculaceae) reflects the geological history of the three great Asian plateaus

Kun-Li Xiang[1,2], Andrey S. Erst[3,4], Jian Yang[1], Huan-Wen Peng[1,2], Rosa del C. Ortiz[5], Florian Jabbour[6], Tatyana V. Erst[4,7] and Wei Wang[1,2]

[1]State Key Laboratory of Systematic and Evolutionary Botany, Institute of Botany, Chinese Academy of Sciences, Beijing 100093, People's Republic of China
[2]College of Life Sciences, University of Chinese Academy of Sciences, Beijing 100049, People's Republic of China
[3]Laboratory of Herbarium, Central Siberian Botanical Garden, Russian Academy of Sciences, Zolotodolinskaya Street 101, Novosibirsk 630090, Russia
[4]Laboratory of Herbarium, Tomsk State University, Tomsk 634050, Russia
[5]Missouri Botanical Garden, 4344 Shaw Blvd, St Louis, MO 63166-0299, USA
[6]Institut de Systématique, Evolution, Biodiversité (ISYEB), Muséum national d'Histoire naturelle, CNRS, Sorbonne Université, EPHE, Université des Antilles, Paris 75005, France
[7]Laboratory of Molecular Plant Pathology, Institute of Cytology and Genetics SB RAS, Prospekt Lavrentyeva 10, Novosibirsk 630090, Russia

KLX, 0000-0002-0800-6015; ASE, 0000-0002-4844-0254; RdCO, 0000-0002-4673-4347; FJ, 0000-0002-7729-1067; WW, 0000-0001-6901-6375

The evolutionary history of organisms with poor dispersal abilities usually parallels geological events. Collisions of the Indian and Arabian plates with Eurasia greatly changed Asian topography and affected regional and global climates as well as biotic evolution. However, the geological evolution of Asia related to these two collisions remains debated. Here, we used *Eranthis*, an angiosperm genus with poor seed dispersal ability and a discontinuous distribution across Eurasia, to shed light on the orogenesis of the Qinghai–Tibetan, Iranian and Mongolian Plateaus. Our phylogenetic analyses show that *Eranthis* comprises four major geographical clades: east Qinghai–Tibetan Plateau clade (I-1), North Asian clade (I-2), west Qinghai–Tibetan Plateau clade (II-1) and Mediterranean clade (II-2). Our molecular dating and biogeographic analyses indicate that within *Eranthis*, four vicariance events correlate well with the two early uplifts of the Qinghai–Tibetan Plateau during the Late Eocene and the Oligocene–Miocene boundary and the two uplifts of the Iranian Plateau during the Middle and Late Miocene. The origin and divergence of the Mongolian Plateau taxa are related to the two uplifts of the Mongolian Plateau during the Middle and Late Miocene. Additionally, our results are in agreement with the hypothesis that the central part of Tibet only reached an altitude of less than 2.3 km at approximately 40 Ma. This study highlights that organismal evolution could be related to the formation of the three great Asian plateaus, hence contributing to the knowledge on the timing of the key tectonic events in Asia.

1. Introduction

The collisions of the Indian Subcontinent with Eurasia in the east and Arabian plate with Eurasia in the west are two important tectonic events in Asia [1]. The India–Eurasia collision started at about 61 Ma [2] and subsequently caused the deformation and uplift of the Qinghai–Tibetan Plateau (QTP) and the eastward lateral extrusion of Indochina [1,3,4]. In addition, the Mongolian Plateau (MP) is usually considered to be the consequence of the far-field effect of the continued India–Eurasia convergence [5]. The Arabia–Eurasia collision started at *ca* 35 Ma and resulted in the deformation and uplift of the Iranian Plateau (IP) region and the westward lateral extrusion

of the Anatolia block [6]. The India–Eurasia and Arabia–Eurasia convergences have usually been regarded as separate collision processes, but they may have interacted by controlling the far-field Cenozoic deformation in Asia [1]. This interaction may have generated a northeast oriented zone of Central Asia right-slip faults (300–400-km wide and greater than 1500-km long), which encompassed the Zagros mountains, Tian Shan and Altai Shan orogens and western Mongolia (electronic supplementary material, figure S1). The uplifts and outward growths of the QTP, IP and MP regions and associated mountain belts have had a profound impact on regional and even global climates and environments [7–10]. Yet, the evolution of these three great Asian plateaus remains considerably controversial and is still poorly understood [1,11,12]. The tectonic events affected biotic evolution; in turn, evolutionary diversifications of organisms might could reflect the geological and related climate changes. However, with few exceptions [13,14], evolutionary studies of Asian organisms have focused on a single plateau, such as the QTP [15,16]. This precludes broad comparisons of the geological evolution of Asian plateaus associated with the India–Eurasia and Arabia–Eurasia collisions as a whole.

Ranunculaceae, commonly known as the buttercup family, is an important herbaceous element of mountain ecosystems in the Northern Hemisphere [17]. The family originated in the Lower Cretaceous and experienced a burst of diversification during the Upper Cretaceous (*ca* 83–74 Ma) [18]. Owing to their seeds with poor dispersal abilities, the ranunculaceous species with follicles are often reported to be geographically highly isolated [18] and have been used to infer East Asian floristic evolution [19,20]. In this study, we focus on the biogeographic diversification of the genus *Eranthis*, an early spring ephemeral, known as winter aconite in Europe. Recent molecular clock estimates suggest a stem age of 56–59 Ma for the genus [18]. *Eranthis* mainly inhabits humid environments under deciduous forests of temperate Eurasia (figure 1*a*). The fruits of *Eranthis* are dehiscent follicles (figure 1*b*). Seeds may be simply gravity dispersed owing to lacking obvious adaptation to wind or animal dispersal, and hence are not expected to disperse over long distance or through physical barriers. The species of the genus are found throughout the Eurasian continent, but their distribution is discontinuous and each species is restricted to a particular biogeographic region, i.e. South Europe, South Turkey, the west and east edges of the QTP, MP or Northeast Asia (figure 1*c*; electronic supplementary material, table S1). Furthermore, species of the genus occur both in lowlands and at high elevations in different geographical regions (electronic supplementary material, figure S2). The present-day distribution of *Eranthis* may be linked to the geological evolution of Asia, especially the formation of the three great Asian plateaus and the extrusion of the Anatolia block.

Given the inferred Late Palaeocene age and extensive Eurasian distribution of the genus, a poor dispersal ability, as well as the restriction of each species to particular biogeographic regions, *Eranthis* is a key biological model to infer the geological history of Asia. Here, we present a molecular phylogeny for *Eranthis* that includes all currently recognized species. By integrating phylogenetic, molecular dating and biogeographic methods, we investigate the historical biogeography of the genus, and thereby aim to illuminate the likely evolutionary histories of the three great Asian plateaus.

2. Material and methods

(a) Samples and sequences

We sampled 34 individuals of *Eranthis* (Cimicifugeae, Ranunculaceae), representing all 12 species (including one undescribed new species) [21]. We included nine species covering all three other genera of Cimicifugeae, as well as three species of Asteropyreae, Caltheae and Adonideae as the outgroups [18]. Materials used in this study were mainly collected from herbarium specimens except for a few from the field. Voucher information and GenBank accession numbers are listed in electronic supplementary material, table S3.

Five DNA regions, including plastid (*trnL-F*, *trnH-psbA*, *matK*, *rbcL*) and nuclear (ITS) loci were sequenced. Laboratory procedures, sequence handling and phylogenetic inference followed Xiang *et al*. [19]. Sequences were aligned using Geneious 10.1.3 [22], and adjusted manually. The final alignments contained 46 taxa with 1001 bp for *trnL-F* (excluding three ambiguous regions with 114 nucleotides), 251 bp for *trnH-psbA* (excluding one ambiguous region with 73 nucleotides), 1210 bp for *matK*, 1263 bp for *rbcL* and 668 bp for ITS. Phylogenetic analyses were conducted using maximum likelihood and Bayesian inference methods in RAxML 8.0 [23] and MrBayes 3.2.1 [24], respectively. The plastid and nuclear datasets were each first analysed independently. As there were no significant topological incongruences (greater than or equal to 70% bootstrap percentage and greater than or equal to 0.95 posterior probability) between plastid and nuclear datasets (electronic supplementary material, figure S3 versus electronic supplementary material, figure S4), all subsequent analyses were performed for the combined five-locus dataset only.

(b) Divergence time estimation

Divergence time was estimated in BEAST 2.4.0 [25]. We set an 83 Ma (95% HPD: 77–88 Ma) constraint for the root, which is the estimated age for the split of Cimicifugeae and Adonideae [18], with a normal distribution. *Palaeoactaea nagelii*, fruits from the Late Palaeocene Almont and Beicegel Creek floras of North Dakota, USA, is close to extant *Actaea* based on fruit size and shape and details of seed morphology and anatomy [26,27]. In accordance with previous studies [18,28,29], we gave a lower bound of 56 Ma for the stem group age of *Actaea*. Dating analyses were conducted under the GTR + I + Γ model for each DNA partition separately. Two independent runs of 100 million generations were carried out, sampling every 5000 generations and discarding the first 25% as burn-in. The maximum clade credibility (MCC) tree with median node ages was produced using TreeAnnotator 2.4.0 [25].

We used Bayes factors [30] calculated by marginal likelihoods derived from path sampling [31] to compare four clock models (strict, exponential, lognormal and random) and then two distinct tree speciation priors (Yule and birth–death). Under the optimal clock model (electronic supplementary material, table S4) and tree prior (electronic supplementary material, table S5), we carried out four dating analyses by using four distinct prior distributions for the calibrating fossil (exponential, lognormal, normal and uniform). These four analyses yielded highly similar time estimates for *Eranthis* (electronic supplementary material, table S6). Bayes factors suggested normal prior distribution as optimal for the calibrating fossil (electronic supplementary material, table S7); results from this analysis were thus reported and used for subsequent analyses. For comparative purposes, we also estimated divergence times using a pruned dataset consisting of 24 taxa (one accession per species). The run strategy was the same as the one for the full-data analysis. Both the full-data and species-level analyses highly agree in time estimates for *Eranthis* (electronic supplementary material, table S6).

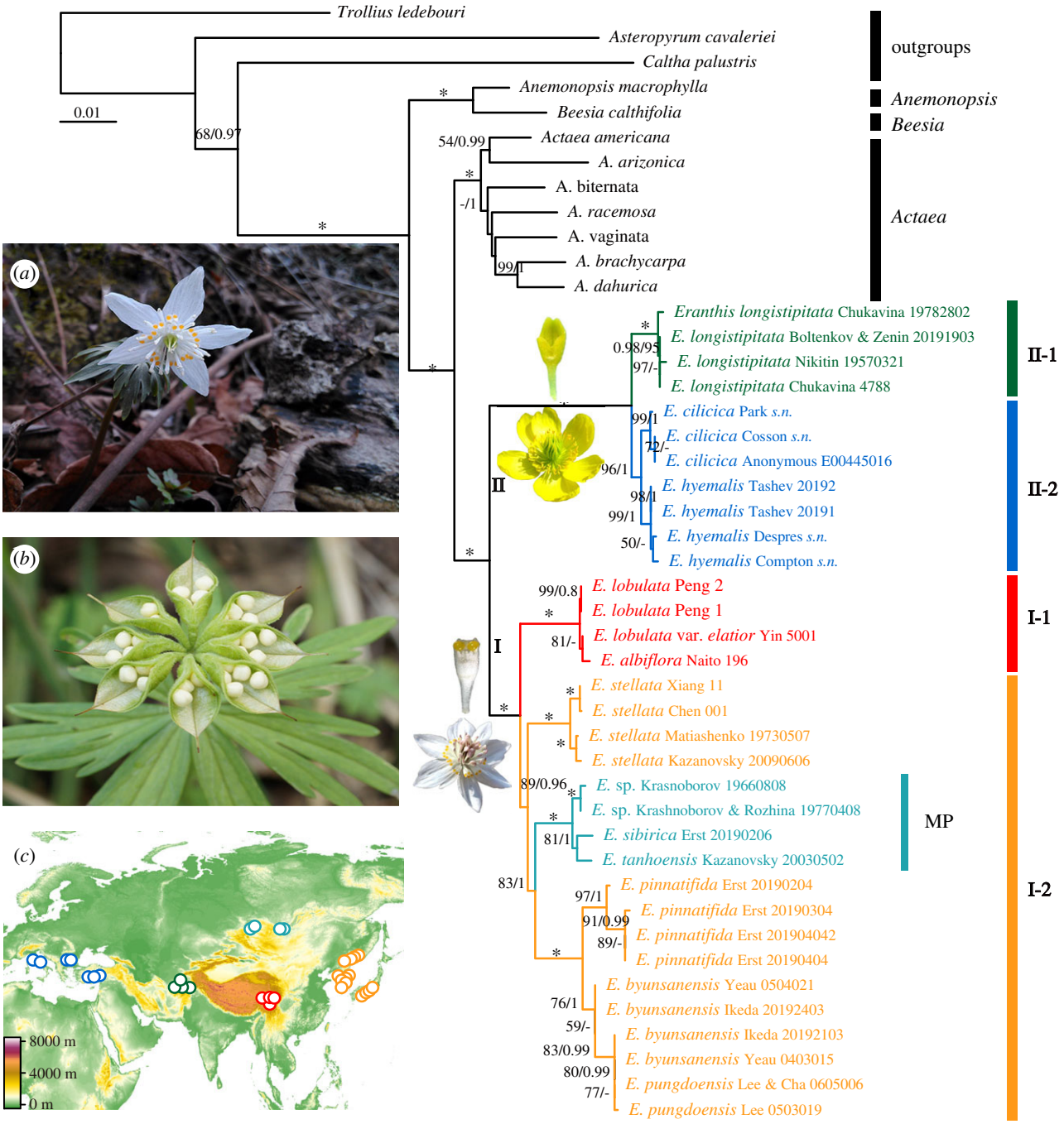

Figure 1. Phylogenetic relationships of *Eranthis* inferred from the combined plastid and nuclear sequences. Numbers above branches are bootstrap values (BS > 50%) and Bayesian posterior probabilities (PP > 0.80). Asterisks indicate BS = 100% and PP = 1.0. (*a*) An early spring *Eranthis* plant under the deciduous forest. (*b*) Dehiscent follicles of *Eranthis*. (*c*) The map shows sampling locations, detailed sampling information is presented in electronic supplementary material, table S3. Photographs by Andrey S. Erst. (Online version in colour.)

To test the robustness of the age estimates, we also used the molecular dataset of *Eranthis* in combination with DNA substitution rate. Four plastid loci were linked in a single clock and a general plastid rate calculated by Zurawski *et al*. [32] was used. A normal distribution with a mean value and standard deviation of 0.001 and 0.0001 were specified in *ucld.mean*. For the nuclear ITS, we selected the substitution rate of herbs used by Wojciechowski *et al*. [33]: a normal distribution with a mean value and standard deviation of 0.0035 and 0.0002. The run settings were the same as the one using the full dataset and the fossil calibration under the optimal prior distribution. The dating results in combination with DNA substitution rate are highly congruent with those that uses only the calibrating fossil (electronic supplementary material, table S8).

(c) Ancestral range reconstruction

We estimated the ancestral ranges of *Eranthis* under the DEC and DIVALIKE models, implemented in the R package BioGeoBEARS [34]. The three outgroups were pruned. Based on the present-day distribution of *Eranthis* and the floristic regions it covers, we defined five bioregions (figure 1*a*): Mediterranean region (including South Europe and the Anatolia peninsula), west QTP, east QTP, Northeast Asia (including eastern Siberia, northeastern China, Korea and Japan) and MP. North America was also coded as a bioregion, in which a few species of *Actaea* occur. We performed the analyses in several different ways: without the maximum number of ancestral areas (maxarea) constrained and with the maxarea constrained to four, three or two. Using the Akaike information criterion, DIVALIKE was selected to be the best-fitting model for each of these four

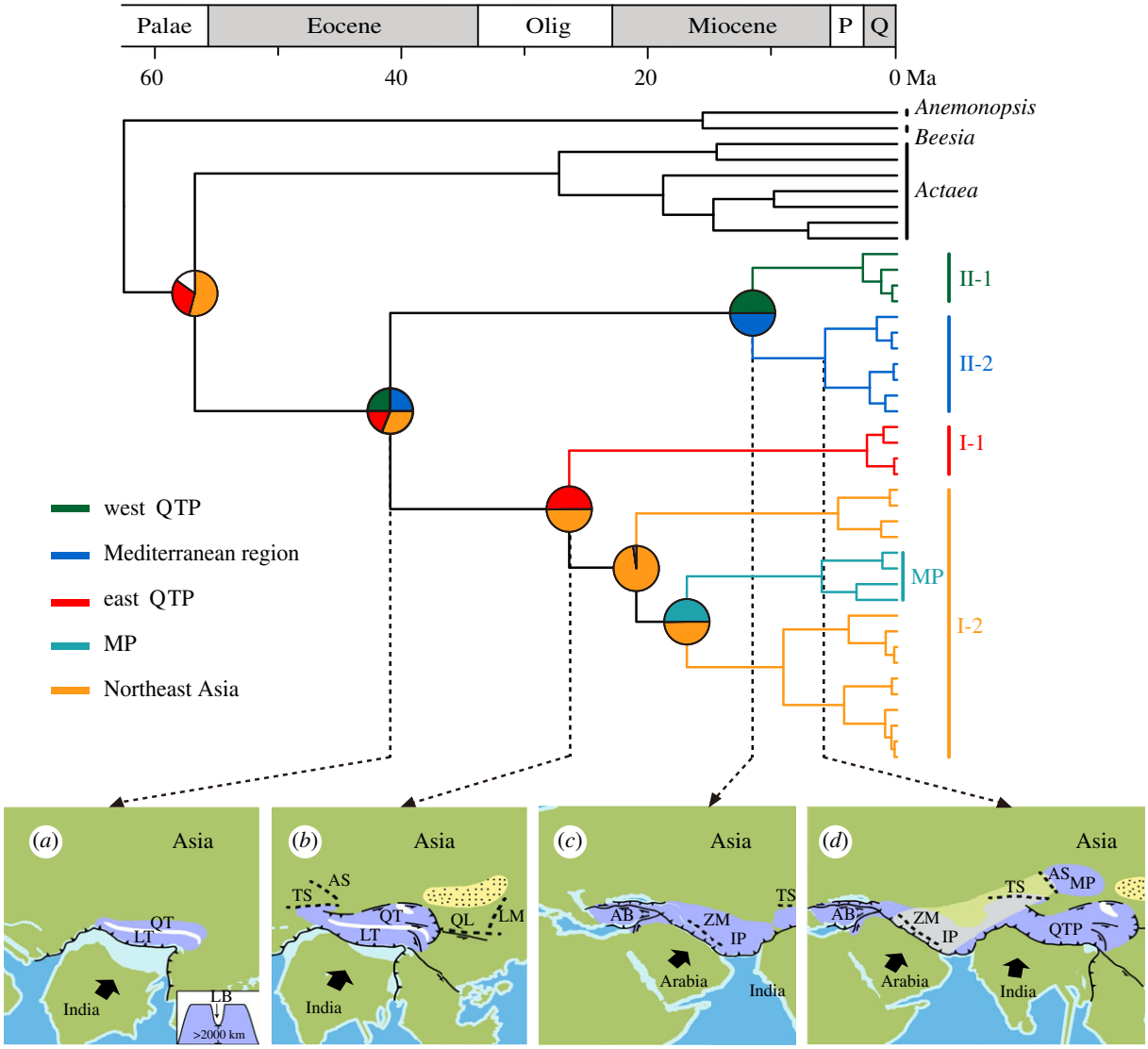

Figure 2. Evolution of *Eranthis* with associated tectonic events. Timetree is modified from the electronic supplementary material, figure S3, generated in BEAST under the best-fitting clock model, tree prior process and fossil prior distribution. Pie charts show the cumulative probabilities for estimated ancestral ranges obtained under the DIVALIKE model, implemented in BioGeoBEARS. (*a*) The QTP region experienced the first uplift around 40 Ma and its central area reached an altitude of less than 2.3 km. (*b*) A second uplift of the QTP region and the resulting adjacent mountain buildings and Asian interior desertification occurred at about 26 Ma. (*c*) Uplift of the IP region and extrusion of the Anatolia block happened at almost the same time, around 12 Ma. (*d*) A second uplift of the IP and MP regions occurred around 6 Ma. The northeast-trending grey area in (*d*) shows the interacted zone between the India–Eurasia and Arabia–Eurasia collisions [1]. A series of palaeo-maps were reconstructed from http://www.odsn.de/odsn/index.html (link 'Plate Tectonic Reconstructions'), and tectonic structures are modified from Yin [1]. AB, Anatolia block; AS, Altai Shan; IP, Iranian Plateau; LB, Lunpola basin; LM, Lüliang mountains; LT, Lhasa terrane; MP, Mongolian Plateau; QL, Qinling; QT, Qiangtang terrane; QTP, Qinghai–Tibetan Plateau; TS, Tian Shan; ZM, Zagros mountains. (Online version in colour.)

analyses (electronic supplementary material, table S9). Under the DIVALIKE model, the results of the four analyses were largely similar based on cumulative ancestral range reconstructions [35]. Each species of *Eranthis* is distributed in one bioregion, the ancestral range reconstruction constraining maxarea to two was thus reported and discussed. To exclude the impact of outgroup areas, we also performed biogeographic analyses by pruning all outgroups. Both biogeographic estimations with or without outgroups entirely agree with the assigned ancestral areas for *Eranthis* (figure 2 versus electronic supplementary material, figure S6).

(d) Ancestral elevation reconstruction

We obtained locality data of the 11 known *Eranthis* species from the following herbaria: B, E, IRK, K, LE, MO, NS, NSK, P, PE, TI and TK (herbarium acronyms follow Index Herbariorum: http://sciweb.nybg.org/science2/Index-Herbariorum.asp), as well as from our field investigations. Localities without accurate coordinates were omitted. In total, we obtained 279 occurrence records with locality information (electronic supplementary material, table S2). For each record, we extracted the elevational variable from the calibration dataset for global land areas at 1-km resolution [36] using the 'raster' function in the 'raster' package of R [37]. The mean and boundaries of the 95% elevational range for each species was then calculated. We inferred the ancestral elevation of *Eranthis* using a squared-change parsimony method in Mesquite 3.61 [38]. This method is relevant for analysing continuous characters [39]. The MCC tree was used and a single accession per species of *Eranthis* was kept. For comparative purposes, we also inferred the ancestral elevation using the phylogenetic independent contrast (PIC) method, which is a Brownian-motion based estimator. The PIC analysis was conducted using the 'ace' function in the 'ape' package of R [33]. These two analytical methods generated highly congruent results (electronic supplementary material, figure S7). The parsimony reconstruction was reported and used for discussion (figure 3).

To test the robustness of the ancestral elevation inferences, we also used elevation information from the literature. The evolutionary reconstructions for boundaries of the elevational interval were carried out using the parsimony method in Mesquite. Both elevation reconstructions using the information extracted based on the occurrence records and from the literature yielded similar results (figure 3 versus electronic supplementary material, figure S8).

3. Results

(a) Phylogeny

Maximum likelihood and Bayesian inference analyses resulted in identical trees (figure 1). Both supported the monophyly of *Eranthis* and recovered *Actaea* as its sister group. *Eranthis* includes two major monophyletic groups (I and II) and four well-supported clades (I-1, east QTP; I-2, North Asia; II-1, west QTP; II-2, Mediterranean), each defined largely by geography. Within clade I-2, the MP taxa clustered together and were nested within a clade of Northeast Asian taxa. The relationships at the species level within *Eranthis* are well resolved (figure 1).

(b) Divergence times

The divergence time estimates for *Eranthis* from the BEAST analysis under the optimal clock model (electronic supplementary material, table S4), tree prior (electronic supplementary material, table S5) and fossil prior distribution (electronic supplementary material, table S7) are shown in figure 2, and more details are provided in electronic supplementary material, figure S3 and electronic supplementary material, table S6. The genus *Eranthis* started to diversify at *ca* 41 Ma (95% highest posterior density (HPD): 25–54 Ma). Within group I, the east QTP taxa (I-1) diverged from the North Asian taxa at *ca* 26 Ma (95% HPD: 14–41 Ma). The split of the MP subclade and its Northeast Asian sister group occurred at *ca* 17 Ma (95% HPD: 8–29 Ma), and the MP subclade diversified around 6 Ma (95% HPD: 2–13 Ma). Diversification of group II occurred at *ca* 12 Ma (95% HPD: 4–24 Ma). The split between southern European and Anatolian species occurred at *ca* 6 Ma (95% HPD: 2–13 Ma).

(c) Ancestral range reconstruction

The ancestral area reconstructions using the DEC and DIVALIKE models in BioGeoBEARS generated highly congruent results, although DIVALIKE was identified as the best-fitting model for our data (electronic supplementary material, table S9). Results under the DIVALIKE model are shown in figure 2. The genus *Eranthis* originated in East Asia, and its most recent common ancestor had likely spread to the west QTP and Mediterranean regions. A subsequent vicariance event led to group I in East Asia and group II in the west QTP, Anatolia and South Europe. Within group I, a vicariance event separated the east QTP clade (I-1) from the North Asian clade (I-2), and a dispersal event from Northeast Asia to the MP within clade I-2 took place. Within group II, a vicariance event isolated the west QTP clade (II-1) and the Mediterranean clade (II-2).

4. Discussion

Our study presents a phylogenetic tree for *Eranthis* with all 12 species (figure 1). Divergence time estimates suggest a crown-group age of 62 Ma (95%HPD: 57–68 Ma) for Cimicifugeae and a stem age of 57 Ma (95%HPD: 53–60 Ma) for *Actaea*, which are consistent with the estimates of Wang *et al*. [18] and Kadereit *et al*. [29], yet they are much older than those of Zhai *et al*. [40]. However, Zhai *et al*. [40] only used the oldest known angiosperm tricolpate pollen as the fossil calibration point to constrain the crown-group age of eudicots and estimated divergence dates within Ranunculaceae. Internal calibrations are regarded critical for obtaining accurate estimates [41]. Detailed comparisons among divergence times estimated in this study and previous studies are shown in electronic supplementary material, table S8.

(a) Spatio-temporal evolution of *Eranthis*

The results of our integrated molecular dating and ancestral range reconstruction analyses (figure 2) indicate that *Eranthis* originated in East Asia, and then dispersed to the west QTP and Mediterranean regions between 56 and 41 Ma. This period is prior to the interruption of the Turgai strait (an epicontinental sea from the Arctic Ocean to the Tethys Seaway) (*ca* 34 Ma) [42] and the demise of the Tarim Sea (an epicontinental sea in the western Tarim Basin of China) (*ca* 34–37 Ma) [43]. Thus, the migration through the north temperate regions of North Asia seems unlikely. A proto-Tibetan highland consisting of the Lhasa and Qiangtang terranes had been assumed to have attained an elevation of greater than 4.5 km before the collision of India with Eurasia, but these two high terranes were at least separated by an east–west oriented elongate lowland along the Bangong–Nujiang suture, represented by a string of basins at present, such as the Lunpola basin [3,8,11,44,45]. Fossil evidence suggests that a humid tropical or subtropical lowland flora existed in the central QTP until the latest Palaeocene to Late Oligocene [9,44,45]. Thus, it is more likely that ancestral populations of *Eranthis* would have migrated westward via this east–west lowland during the Eocene (figure 2*a*).

The spatio-temporal evolution of *Eranthis* may have resulted from the uplifts of the three great Asian plateaus and associated mountain belts, as well as associated environmental changes. The uplift of the QTP region induced by the India–Eurasia collision might have prevented the migration of *Eranthis* through the east–west lowland and thereby resulted in the deep divergence between groups I and II at *ca* 41 Ma (95% HPD: 25–54 Ma). Later, the QTP grew continuously upward and outward and caused the formation of Lüliang and Qinling orogens in the northeast [46,47] and northern Chinese desertification [48]. These events could have caused the extinction of *Eranthis* in the northern and central China and thereby resulted in the split between clades I-1 and I-2 around 26 Ma (95% HPD: 14–41 Ma). Contrary to the Northeast Asian taxa, the east QTP taxa are distributed at higher elevations (figure 3). Our analyses recovered one dispersal from Northeast Asia to the MP, suggesting Northeast Asia as the source for the MP biodiversity. The split between the MP subclade and its Northeast Asian sister group at *ca* 17 Ma (95% HPD: 8–29 Ma) is likely related to the uplift of the MP region, which was suggested to be the consequence of the far-field effect of the India–Eurasia and Arabia–Eurasia collisions [1]. The divergence of the west QTP clade (II-1) from the Mediterranean taxa (II-2) around 12 Ma (95% HPD: 4–24 Ma) is probably linked to the uplift of the IP region and the extrusion of the Anatolia block resulting from the Arabia–Eurasia collision.

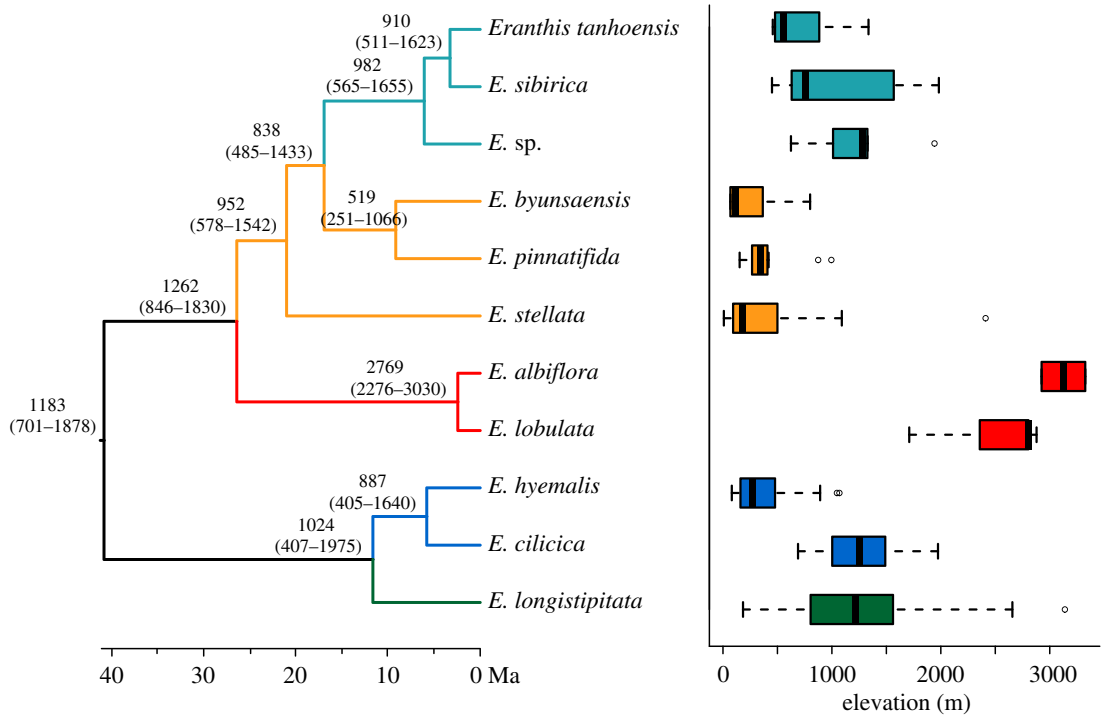

Figure 3. Ancestral reconstruction of the mean and boundaries of the 95% elevational range using Mesquite. Box and whisker plot indicates the elevational range of each species. Numbers above the branches are the mean and boundaries of the 95% elevational range (in metres) for ancestral nodes. Branch colours correspond to the four clades presented in figure 1. (Online version in colour.)

(b) Biogeographic implications for the geological evolution of Asia

Because of its conserved habitat, poor dispersal ability and scattered geographical distribution across Eurasia, *Eranthis* possesses unique genetic imprints that reflect the history of geological and environmental changes in Asia during the Cenozoic.

Following the initial India–Eurasia collision in the Early Cenozoic (*ca* 61 Ma) [2], the uplift and outward growth of the QTP occurred and continued well into the Miocene [8]. The deep divergence between the east and west groups (I and II) took place in the central part of the QTP around 41 Ma, associated with the first uplift of the QTP (figure 2*a*). This time frame is in concert with the results of geological studies, which indicate that the east and central QTP and its northern margin were elevated around 40 Ma [49–51]. The origin of alpine ginger [52] and the divergence of west Chinese salamanders [53] were estimated to have occurred during the same period, both of which were also suggested to be related to this uplift of the QTP region. The palaeoelevational estimate for the hinterland of the QTP, i.e. a string of basins between the Lhasa and Qiangtang terranes, is crucial for understanding Tibetan landscape evolution, but has been intensely debated [1,9,11]. Our elevation reconstructions suggest that the most recent common ancestor of *Eranthis* likely occurred up to the highest altitude of about 1.8 km (figure 3). Accordingly, we hypothesize that after the first uplift (*ca* 40 Ma), the central QTP likely had an elevation of less than 2 km, likely about 1.8 km (figure 2*a*). This differs from the hypothesis that during the first uplift the QTP reached an altitude of at least 2.5 km [53]. Our estimate is compatible with the result of the magnetostratigraphic and radiochronologic dating that indicates that the elevations of central Tibet were generally low (less than 2.3 km) at 39.5 Ma [45]. Also, the palaeobotanical evidence suggests an elevation of less than 2.3 km for the Lunpola basin of central QTP at *ca* 25 Ma [11] and an elevation of 1.5–2.9 km for the Kailas Basin in the western part of the Lhasa terrane during the latest Oligocene [54].

The split between the east QTP clade (I-1) and the North Asian clade (I-2) (figure 2*b*; *ca* 26 Ma) suggests a second uplift of the QTP region and the resulting palaeoclimatic changes. This age fell in line with the deep splits of lineages in alpine ginger (*ca* 32 Ma, 95% HPD: 18–50 Ma) [52] and in spiny frogs (*ca* 27 Ma, 95% HPD: 19–36 Ma) [55], both of which were postulated to have been triggered by this rapid uplift. A few endemic plant genera of the QTP, such as *Nannoglottis* (Asteraceae) [56] and *Gymnaconitum* (Ranunculaceae) [57] also originated during this period. This uplift has not only significantly modified Asian physiognomy, but has also greatly affected the regional and even the global climate and biotic evolution [9,49]. During this period, the QTP extended outward and consequently gave rise to adjacent mountain buildings by a far-field effect, such as the Emei mountain in the east [58] and Lüliang and Qinling mountains in the northeast [46,47], the onset of Asian interior desertification (*ca* 25 Ma) [48] and the establishment of East Asian monsoon climate [59]. Palaeontological evidence shows that radical changes in vegetation and biotic components occurred in the TP and adjacent regions around the Oligocene–Miocene transition [9,60].

The split between the west QTP clade (II-1) and the Mediterranean clade (II-2) (figure 2*c*; *ca* 12 Ma) suggests a rapid uplift of the IP region triggered by the Arabia–Eurasia collision, which served slab detachment in eastern Turkey and northwestern Zagros [6]. Our dating is highly consistent with the geological hypothesis that uplift, exhumation and shortening in the Zagros mountains and the IP region accelerated at about 15–12 Ma [6]. The Arabia–Eurasia collision displaced the Anatolia block westward relative to the IP,

which occurred at about 15–11 Ma [61] or 7–5 Ma [62,63]. Contrary to the eastward lateral extrusion of Indochina that has been widely investigated [52,55,64], the westward lateral extrusion of the Anatolia block has yet to be examined using modern phylogenetic and biogeographic methods. Our data suggest that the uplift and tectonic extrusion should have occurred synchronously to generate the observed distribution pattern in *Eranthis* around 12 Ma (figure 2*c*). The split between the Anatolian and southern European species was estimated at *ca* 6 Ma, associated with the progressive uplift and expansion of the IP region. This is supported by geological studies, indicating an about 7–8 Ma uplift of the southern margin of the Anatolia block [65] and an about 5 Ma active mountain building of the Zagros mountains [66].

The split of the MP subclade and its Northeast Asian sister group occurred at about 17 Ma. The species in the MP are distributed at relatively higher elevations than the species in the Northeast Asia (figure 3). We hypothesize that the split was associated with geological events that separated the MP and Northeast Asia. Our estimated age is compatible with the geological hypothesis that the rapid uplift of the MP region occurred around 20–10 Ma [67,68]. The diversification of the MP subclade arose at about 6 Ma (figure 2*d*), which implies a second uplift and expansion of the MP region. This hypothesis is consistent with the geological hypotheses that the summit of the MP emerged at about 5–10 Ma [69] and that the uplift of the Gobi-Altai mountain range of Mongolia started at 5 ± 3 Ma [5]. The two discrete intervals of uplift of the MP region that our analyses revealed are concurrent with those of the rapid uplift and expansion of the QTP and IP regions (figure 2*b*,*c*) [6,69,70], and with those of the Tian Shan and Altai Shan [71,72]. The MP, Tian Shan and Altai Shan are all located in the Central Asian right-slip fault zone (electronic supplementary material, figure S1) [1]. Thus, we suggest that the two uplifts of the MP region in the Miocene likely represent two rapid responses to the interaction of the India–Eurasia and Arabia–Eurasia collisions.

In conclusion, our study provides the first case, to our knowledge, of an organismal group reconciling and illuminating the geological history of the QTP, IP and MP. The biogeography of *Eranthis* may have been shaped by multiple uplifts of these three Asian plateaus and the extrusion of the Anatolia block. Considering the wide credibility intervals of the estimated times of divergence, we urge caution interpreting these results and the geological hypotheses that we put forward should be further tested by studying other taxa that exhibit similar habitat requirements and dispersal abilities in Eurasia.

Data accessibility. The sequences reported in this paper have been deposited in the GenBank database (accession nos. MW716473–MW716501; MW722251–MW722357). The datasets supporting this article are available from the Dryad Digital Repository: https://doi.org/10.5061/dryad.0zpc866wz [73].

Authors' contributions. W.W. conceived the research. K.-L.X., A.S.E., H.-W.P., R.d.C.O., F.J. and T.V.E. carried out taxon sampling. K.-L.X., A.S.E. and J.Y. generated all the data. K.-L.X., A.S.E., J.Y., H.-W.P. and W.W. performed the data analyses. W.W. led the writing with contributions from all co-authors.

Competing interests. We declare we have no competing interests.

Funding. This work was supported by the Strategic Priority Research Program of Chinese Academy of Sciences (grant no. XDB31000000), the National Natural Science Foundation of China (grant nos. 31770231, 31770233 and 32011530072), K.C.Wong Education Foundation (grant no. GJTD-2020-05) and the Russian Science Foundation (grant no. 19-74-10082).

Acknowledgements. We thank the associated editor and two anonymous reviewers for constructive comments which greatly improved this manuscript. We thank Cynthia Hong Wa for reading an early draft of the manuscript and Xiao-Guo Xiang for critical comments on the manuscript.

References

1. Yin A. 2010 Cenozoic tectonic evolution of Asia: a preliminary synthesis. *Tectonophysics* **488**, 293–325. (doi:10.1016/j.tecto.2009.06.002)
2. Yuan J, Yang Z, Deng C, Krijgsman W, Zhu R. 2020 Rapid drift of the Tethyan Himalaya terrane before two-stage India-Asia collision. *Nat. Sci. Rev.* nwaa173 (doi:10.1093/nsr/nwaa173)
3. Spicer RA, Su T, Valdes PG, Farnsworth A, Wu FX, Shi GL, Spicer TEV, Zhou ZK. 2021 Why the 'uplift of the Tibetan Plateau' is a myth. *Nat. Sci. Rev.* **8**, nwaa091 (doi:10.1093/nsr/nwaa1091)
4. Tapponnier P *et al.* 1990 The Ailao Shan/Red River metamorphic belt: tertiary left-lateral shear between Indochina and South China. *Nature* **343**, 431–437. (doi:10.1038/343431a0)
5. Vassallo R, Joliveta M, Ritza JF, Braucher R, Larroque C, Sue C, Todbileg M, Javkhlanbold D. 2007 Uplift age and rates of the Gurvan Bogd system (Gobi-Altay) by apatite fission track analysis. *Earth Planet Sci. Lett.* **259**, 333–346. (doi:10.1016/j.epsl.2007.04.047)
6. Mouthereau F, Lacombe O, Vergés J. 2012 Building the Zagros collisional orogen: timing, strain distribution and the dynamics of Arabia/Eurasia plate convergence. *Tectonophysics* **27–60**, 532–535. (doi:10.1016/j.tecto.2012.01.022)
7. Farnsworth A, Lunt DJ, Robinson SA, Valdes PJ, Pancost RD. 2019 Past East Asian monsoon evolution controlled by paleogeography, not CO_2. *Sci. Adv.* **5**, eaax1697. (doi:10.1126/sciadv.aax1697)
8. Spicer RA, Farnsworth A, Su T. 2020 Cenozoic topography, monsoons and biodiversity conservation within the Tibetan Region: an evolving story. *Plant Divers* **42**, 229–254. (doi:10.1016/j.pld.2020.06.011)
9. Deng T, Wu F, Wang S, Su T, Zhou Z. 2021 Major turnover of biotas across the Oligocene/Miocene boundary on the Tibetan Plateau. *Palaeogeogr. Palaeoclimatol. Palaeoecol.* **567**, 11241. (doi:10.1016/j.palaeo.2021.110241)
10. Li SF *et al.* 2021 Orographic evolution of northern Tibet shaped vegetation and plant diversity in eastern Asia. *Sci. Adv.* **7**, eabc7741. (doi:10.1126/sciadv.abc7741)
11. Su T *et al.* 2019 No high Tibetan Plateau until the Neogene. *Sci. Adv.* **5**, eaav2189. (doi:10.1126/sciadv.aav2189)
12. Renner SS. 2016 Available data point to a 4-km-high Tibetan Plateau by 40 Ma, but 100 molecular-clock papers have linked supposed recent uplift to young node ages. *J. Biogeogr.* **43**, 1479–1487. (doi:10.1111/jbi.12755)
13. Jabbour F, Renner S. 2012 A phylogeny of Delphinieae (Ranunculaceae) shows that *Aconitum* is nested within *Delphinium* and that Late Miocene transitions to long life cycles in the Himalayas and southwest China coincide with bursts in diversification. *Mol. Phylogenet. Evol.* **62**, 928–942. (doi:10.1016/j.ympev.2011.12.005)
14. Manafzadeh S, Salvo G, Conti E. 2013 A tale of migrations from east to west: the Irano-Turanian floristic region as a source of Mediterranean xerophytes. *J. Biogeogr.* **41**, 366–379. (doi:10.1111/jbi.12185)
15. Favre A, Päckert M, Pauls SU, Jähnig SC, Uhl D, Michalak I, Muellner-Riehl AN. 2015 The role of the uplift of the Qinghai–Tibetan Plateau for the evolution of Tibetan biotas. *Biol. Rev.* **90**, 236–253. (doi:10.1111/brv.12107)

16. Zhao Z, Li S. 2017 Extinction vs. rapid radiation: the juxtaposed evolutionary histories of coelotine spiders support the Eocene–Oligocene orogenesis of the Tibetan Plateau. *Syst. Biol.* **66**, 988–1006. (doi:10.1093/sysbio/syx042)
17. Ziman SN, Keener CS. 1989 A geographical analysis of the family Ranunculaceae. *Ann. MO. Bot. Gard.* **76**, 1012–1049. (doi:10.2307/2399690)
18. Wang W, Lin L, Xiang XG, Ortiz RDC, Liu Y, Xiang KL, Yu SX, Xing YW, Chen ZD. 2016 The rise of angiosperm-dominated herbaceous floras: insights from Ranunculaceae. *Sci. Rep.* **6**, 27259. (doi:10.1038/srep27259)
19. Xiang KL, Zhao L, Erst AS, Yu SX, Jabbour F, Wang W. 2017 A molecular phylogeny of *Dichocarpum* (Ranunculaceae): implications for eastern Asian biogeography. *Mol. Phylogenet. Evol.* **107**, 594–604. (doi:10.1016/j.ympev.2016.12.026)
20. Xiang KL, Erst AS, Xiang XG, Jabbour F, Wang W. 2018 Biogeography of *Coptis* Salisb. (Ranunculales, Ranunculaceae, Coptidoideae), an Eastern Asian and North American genus. *BMC Evol. Biol.* **18**, 74. (doi:10.1186/s12862-018-1195-0)
21. Erst AS *et al*. 2020 An integrative taxonomic approach reveals a new species of *Eranthis* (Ranunculaceae) in North Asia. *PhytoKeys* **140**, 75–100. (doi:10.3897/phytokeys.140.49048)
22. Kearse M *et al*. 2012 Geneious basic: an integrated and extendable desktop software platform for the organization and analysis of sequence data. *Bioinformatics* **28**, 1647–1649. (doi:10.1093/bioinformatics/bts199)
23. Stamatakis A. 2014 RAxML version 8: a tool for phylogenetic analysis and post-analysis of large phylogenies. *Bioinformatics* **30**, 1312–1313. (doi:10.1093/bioinformatics/btu033)
24. Ronquist F *et al.* 2012 MrBayes 3.2: efficient Bayesian phylogenetic inference and model choice across a large model space. *Syst. Biol.* **61**, 539–542. (doi:10.2307/41515220)
25. Bouckaert R, Heled J, Kühnert D, Vaughan T, Wu CH, Xie D, Suchard MA, Rambaut A, Drummond AJ. 2014 BEAST 2: a software platform for Bayesian evolutionary analysis. *PLoS Comput. Biol.* **10**, e1003537. (doi:10.1371/journal.pcbi.1003537)
26. Pigg KB, DeVore ML. 2005 *Paleoactaea* gen. nov (Ranunculaceae) fruits from the Paleogene of North Dakota and the London clay. *Am. J. Bot.* **92**, 1650–1659. (doi:10.3732/ajb.92.10.1650)
27. Stevens PF. 2001 onwards Angiosperm Phylogeny Website. Version 14, July 2017. See http://www.mobot.org/MOBOT/research/APweb/ (accessed 10 Jun 2020).
28. Chen J, Xie L. 2014 Molecular phylogeny and historical biogeography of *Caltha* (Ranunculaceae) based on analyses of multiple nuclear and plastid sequences. *J. Syst. Evol.* **52**, 51–67. (doi:10.1111/jse.12051)
29. Kadereit JW, Lauterbach M, Kandziora M, Spillmann J, Nyffeler R. 2019 Dual colonization of European high-altitude areas from Asia by *Callianthemum* (Ranunculaceae). *Plant Syst. Evol.* **305**, 431–443. (doi:10.1007/s00606-019-01583-5)
30. Kass RE, Raftery AE. 1995 Bayes factors. *J. Am. Stat. Assoc.* **90**, 773–795. (doi:10.1080/01621459.1995.10476572)
31. Baele G, Li WLS, Drummond AJ, Suchard MA, Lemey P. 2013 Accurate model selection of relaxed molecular clocks in Bayesian phylogenetics. *Mol. Biol. Evol.* **30**, 239–243. (doi:10.1093/molbev/mss243)
32. Zurawski G, Clegg MT, Brown AHD. 1984 The nature of nucleotide sequence divergence between barley and maize chloroplast DNA. *Genetics* **106**, 735–749. (doi:10.1093/genetics/106.4.735)
33. Wojciechowski MF, Sanderson MJ, Hu JM. 1999 Evidence on the monophyly of *Astragalus* (Fabaceae) and its major subgroups based on nuclear ribosomal DNA ITS and chloroplast DNA *trnL* intron data. *Syst. Bot.* **24**, 409–437. (doi:10.2307/241969)
34. Matzke NJ. 2013 Probabilistic historical biogeography: new models for founder-event speciation, imperfect detection, and fossils allow improved accuracy and model-testing. *Front. Biogeogr.* **5**, 242–248. (doi:10.21425/F5FBG19694)
35. Ebersbach J, Muellner-Riehl AN, Michalak I, Tkach N, Hoffmann MH, Röser M, Sun H, Favre A. 2016 In and out of the Qinghai–Tibet Plateau: divergence time estimation and historical biogeography of the large arctic-alpine genus *Saxifraga* L. *J. Biogeogr.* **44**, 900–910. (doi:10.1111/jbi.12899)
36. Ficka SE, Hijmans RJ. 2017 WorldClim 2: new 1-km spatial resolution climate surfaces for global land areas. *Int. J. Climatol.* **37**, 4302–4315. (doi:10.1002/joc.5086)
37. Hijmans RJ. 2020 raster: Geographic data analysis and modeling. R package version 3.1-5. See http://CRAN.R-project.org/package=raster (accessed Aug 2020).
38. Maddison WP, Maddison DR. 2019 Mesquite: A modular system for evolutionary analysis. Version 3.61. See http://mesquiteproject.org (accessed Aug 2020).
39. Paradis E, Claude J, Strimmer K. 2004 APE: analyses of phylogenetics and evolution in R language. *Bioinformatics* **20**, 289–290. (doi:10.1093/bioinformatics/btg412)
40. Zhai W, Duan X, Zhang R, Guo C, Li L, Xu G, Shan H, Kong H, Ren Y. 2019 Chloroplast genomic data provide new and robust insights into the phylogeny and evolution of the Ranunculaceae. *Mol. Phylogenet. Evol.* **135**, 12–21. (doi:10.1016/j.ympev.2019.02.024)
41. Yang ZH, Rannala B. 2006 Bayesian estimation of species divergence times under a molecular clock using multiple fossil calibrations with soft bounds. *Mol. Biol. Evol.* **23**, 212–226. (doi:10.1093/molbev/msj024)
42. Tiffney BH. 1985 Perspectives on the origin of the floristic similarity between eastern Asia and eastern North America. *J. Arn. Arb.* **66**, 73–94. (doi:10.5962/bhl.part.13179)
43. Bosboom RE *et al*. 2011 Late Eocene sea retreat from the Tarim Basin (West China) and concomitant Asian paleoenvironmental change. *Palaeogeogr. Palaeoclimatol. Palaeoecol.* **299**, 385–398. (doi:10.1016/j.palaeo.2010.11.019)
44. Su T *et al*. 2020 A Middle Eocene lowland humid subtropical 'Shangri-La' ecosystem in central Tibet. *Proc. Natl Acad. Sci. USA* **117**, 32 989–32 995. (doi:10.1073/pnas.2012647117)
45. Fang X *et al.* 2020 Revised chronology of central Tibet uplift (Lunpola Basin). *Sci. Adv.* **6**, eaba7298. (doi:10.1126/sciadv.aba7298)
46. Li JX, Yue LP, Liu CY, Wang X, Li G. 2013 The tectonic–sedimentary evolution of the Lüliang mountains since the Miocene. *J. Stratigr.* **37**, 93–100.
47. Wang B, Chang H, Duan KQ. 2017 The tectonic uplift and its environmental effects of the Qinling Mountains during the Cenozoic Era: progress and problems. *Adv. Earth Sci.* **32**, 707–715. (doi:10.11867/j.issn.1001-8166.2017.07.0707)
48. Qiang X *et al*. 2011 New eolian red clay sequence on the western Chinese Loess Plateau linked to onset of Asian desertification about 25 Ma ago. *Sci. China Earth Sci.* **54**, 136–144. (doi:10.1007/s11430-010-4126-5)
49. Chung SL, Lo CH, Lee TY, Zhang YQ, Xie YW, Li XH, Wang KL, Wang PL. 1998 Diachronous uplift of the Tibetan plateau starting 40 Myr ago. *Nature* **394**, 769–773. (doi:10.1038/29511)
50. Wang CS *et al.* 2008 Constraints on the early uplift history of the Tibetan Plateau. *Proc. Natl Acad. Sci. USA* **105**, 4987–4992. (doi:10.1073/pnas.0703595105)
51. Shi W, Wang F, Wu L, Yang L, Zhang W, Wang Y. 2018 A prolonged Cenozoic erosional period in East Kunlun (Western China): constraints of detrital apatite (U-Th)/He ages on the onset of mountain building along the northern margin of the Tibetan Plateau. *J. Asian Earth Sci.* **151**, 54–61. (doi:10.1016/j.jseaes.2017.10.027)
52. Zhao JL, Xia YM, Cannon CH, Kress WJ, Li QJ. 2016 Evolutionary diversification of alpine ginger reflects the early uplift of the Himalayan–Tibetan Plateau and rapid extrusion of Indochina. *Gondwana Res.* **32**, 232–241. (doi:10.1016/j.gr.2015.02.004)
53. Zhang P, Chen YQ, Zhou H, Liu YF, Wang XL, Papenfuss TJ, Wake DB, Qu LH. 2006 Phylogeny, evolution, and biogeography of Asiatic salamanders (Hynobiidae). *Proc. Natl Acad. Sci. USA* **103**, 7360–7365. (doi:10.1073/pnas.0602325103)
54. Ai K, Shi G, Zhang K, Ji J, Guo SX. 2019 The uppermost Oligocene Kailas flora from southern Tibetan Plateau and its implications for the uplift history of the southern Lhasa terrane. *Palaeogeogr. Palaeoclimatol. Palaeoecol.* **515**, 143–151. (doi:10.1016/j.palaeo.2018.04.017)
55. Che J, Zhou WW, Hu JS, Yan F, Papenfuss TJ, Wake DB, Zhang YP. 2010 Spiny frogs (Paini) illuminate the history of the Himalayan region and southeast Asia. *Proc. Natl Acad. Sci. USA* **107**, 13 765–13 770. (doi:10.1073/pnas.1008415107)
56. Liu JQ, Gao TG, Chen ZD, Lu AM. 2002 Molecular phylogeny and biogeography of the Qinghai–Tibet Plateau endemic *Nannoglottis* (Asteraceae). *Mol.*

Phylogenet. Evol. **23**, 307–325. (doi:10.1016/S1055-7903(02)00039-8)

57. Wang W, Liu Y, Yu S, Gao T, Chen Z. 2013 *Gymnaconitum*, a new genus of Ranunculaceae endemic to the Qinghai–Tibetan Plateau. *Taxon* **62**, 713–722. (doi:10.12705/624.10)
58. Meng K, Wang E, Wang G. 2016 Uplift of the Emei Shan, western Sichuan Basin: Implication for eastward propagation of the Tibetan Plateau in Early Miocene. *J. Asian Earth Sci.* **115**, 29–39. (doi:10.1016/j.jseaes.2015.09.020)
59. Ding W, Hou D, Gan J, Wu P, Zhang M, George SC. 2021 Palaeovegetation variation in response to the late Oligocene-early Miocene East Asian summer monsoon in the Ying-Qiong Basin, South China Sea. *Palaeogeogr. Palaeoclimatol. Palaeoecol.* **567**, 110205. (doi:10.1016/j.palaeo.2020.110205)
60. Sun X, Wang P. 2005 How old is the Asian monsoon system? Palaeobotanical records from China. *Palaeogeogr. Palaeoclimatol. Palaeoecol.* **222**, 181–222. (doi:10.1016/j.palaeo.2005.03.005)
61. Sengör AMC, Tuysuz O, Imren C, Sakınç M, Eyidoğan H, Görür N, Pichon XL, Rangin C. 2005 The North anatolian fault: a new look. *Annu. Rev. Earth Planet Sci.* **33**, 37–112. (doi:10.1146/annurev.earth.32.101802.120415)
62. Westaway R. 2004 Kinematic consistency between the Dead Sea Fault Zone and the Neogene and Quaternary left-lateral faulting in SE Turkey. *Tectonophys* **391**, 203–237. (doi:10.1016/j.tecto.2004.07.014)
63. Hubert-Ferrari A, Armijo R, King G, Meyer B, Barka A. 2002 Morphology, displacement, and slip rates along the North Anatolian Fault, Turkey. *J. Geophys. Res.* **107**, 101 029–101 059. (doi:10.1029/2001JB000393)
64. Luo YF, Li SQ. 2017 Caver *Stedocys* spitting spiders illuminate the history of the Himalayas and southeast Asia. *Ecography* **41**, 414–423. (doi:10.1111/ecog.02908)
65. Meijers MJM, Brocard GY, Cosca MC, Ludecke T, Teyssier C, Whitney DL, Andreas M. 2018 Rapid late Miocene surface uplift of the Central Anatolian Plateau margin. *Earth Planet Sci. Lett.* **497**, 29–41. (doi:10.1016/j.epsl.2018.05.040)
66. Lacombe O, Mouthereau F, Kargar S, Meyer B. 2006 Late Cenozoic and modern stress fields in the western Fars (Iran): implications for the tectonic and kinematic evolution of central Zagros. *Tectonics* **25**, TC1003. (doi:10.1029/2005TC001831)
67. Smith SG, Wegmann KW, Ancuta LD, Gosse JC, Hopkins CE. 2016 Paleotopography and erosion rates in the central Hangay Dome, Mongolia: landscape evolution since the mid-Miocene. *J. Asian Earth Sci.* **125**, 37–57. (doi:10.1016/j.jseaes.2016.05.013)
68. Feng LX, Brown RW, Han BF, Wang ZZ, Luszczak K, Liu B, Zhang ZC, Ji JQ. 2017 Thrusting and exhumation of the southern Mongolian Plateau: joint thermochronological constraints from the Langshan Mountains, western Inner Mongolia, China. *J. Asian Earth Sci.* **144**, 287–302. (doi:10.1016/j.jseaes.2017.01.001)
69. Kurushin RA, Bayasgalan A, Ölziybat M, Enhtuvshin B, Molnar P, Bayarsayhan C, Hudnut KW, Lin J. 1998 The surface rupture of the 1957 Gobi–Altay, Mongolia, earthquake. *Geol. Soc. Am. Spec. Pap.* **320**, 1–144. (doi:10.1130/0-8137-2320-5.1)
70. Hodell DA, Mueller PA, Garrido JR. 1991 Variations in the strontium isotopic composition of seawater during the Neogene. *Geology* **19**, 24–27. (doi:10.1130/0091-7613(1991)0192.3.CO)
71. Caves JK, Bayshashov BU, Zhamangara A, Ritch AJ, Ibarra DE, Sjostrom DJ, Mix HT, Winnick MJ, Chamberlain CP. 2017 Late Miocene uplift of the Tian Shan and Altai and reorganization of Central Asia climate. *GSA Today* **27**, 19–26. (doi:10.1130/GSATG305A.1)
72. Wang LN, Ji JQ, Sun DX, Xu QQ, Tu JY, Zhang ZC, Han BF. 2010 The uplift history of south-western Tian Shan: implications from AFT analysis of detrital samples. *Chin. J. Geophys.* **53**, 931–945. (doi:10.3969/j.issa0001-5733.2010.04.018)
73. Xiang K-L, Erst AS, Yang J, Peng H-W, Ortiz R del C, Jabbour F, Erst TV, Wang W. 2021 Data from: Biogeographic diversification of *Eranthis* (Ranunculaceae) reflects the geological history of the three great Asian plateaus. Dryad Digital Repository. (doi:10.5061/dryad.0zpc866wz)